RSC Advances

ROYAL SOCIETY OF CHEMISTRY

www.rsc.org/advances

Graphical abstract

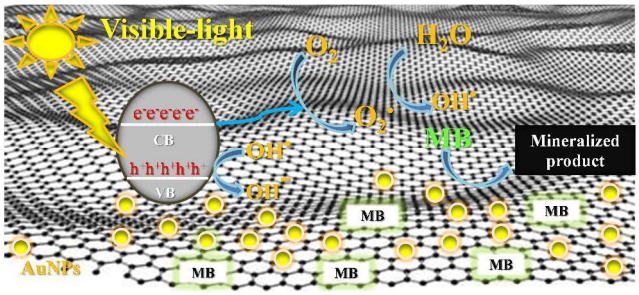

Visible light-induced photocatalytic degradation of pollutants using Au-Graphene nanocomposite.

Journal Name

RSC Publishing

ARTICLE

Green Synthesis, Photocatalytic and Photoelectrochemical Performance of Au-Graphene Nanocomposite†

Cite this: DOI: 10.1039/x0xx00000x

Mohammad Ehtisham Khan[1], Mohammad Mansoob Khan[1,2]*, and Moo Hwan Cho[1]*

Received 00th January 2012,
Accepted 00th January 2012

DOI: 10.1039/x0xx00000x

www.rsc.org/

A simplistic and environment friendly approach using electrochemically active biofilms (EABs) was developed for the synthesis of Au-Graphene (Au-G) nanocomposite without the use of surfactants or capping agents. The as-prepared Au-G nanocomposite was characterized by X-ray diffraction, diffuse reflectance spectroscopy, Raman spectroscopy, X-ray photoelectron spectroscopy, photoluminescence spectroscopy, and transmission electron microscopy. In this study, the anchoring of gold nanoparticles (AuNPs) on graphene sheets was achieved using an EAB. The EAB assists in the bio-reduction of Au^{3+} to Au^{0}, and the AuNPs prevent the aggregation of graphene sheets and keep them apart because of the decrease in attractive forces between the graphene layers. The photocatalytic activities of the Au-G nanocomposite were evaluated by the photocatalytic degradation of methylene blue in an aqueous solution at ambient temperature in the dark and under visible-light irradiation. The photocatalytic activity of the Au-G nanocomposite was enhanced significantly by the loading of AuNPs onto graphene sheets. The photocurrent of the Au-G nanocomposite was measured by linear sweep voltammetry, which exhibited much better performance than pure graphene. The high photocatalytic activity and photocurrent of Au-G nanocomposite was attributed mainly to the anchoring of AuNPs on the graphene sheets. The synergistic effects of the surface plasmonic resonance of AuNPs and the specific electronics effect of graphene holds great promise for the development of electrochemical devices. Therefore, the Au-G nanocomposite has potential in several fields, such as photocatalysis, photovoltaic, nanoelectronics, ultracapacitors, and sensors because of the enhanced photocatalytic and photoelectrochemical performance.

Introduction

Water purification has become a worldwide problem, particularly, in industrialized countries, where wastewater normally contains organic pollutants, such as organic dyes from the textile industry, organic waste materials from the leather and tanning industry, paper industry, food industry, agricultural research, and pharmaceutical industry.[1-3] The release of these colored compounds in the environment has raised considerable concern because of their toxic effects in the environment. In addition, two families of dyes, azo dyes and thiazine dyes can cause serious health risks. Some azo dyes are highly carcinogenic.[2,3] The conventional wastewater treatment plants cannot degrade the majority of these pollutants. Hence, there has been increasing interest in methods for the decontamination over the past few decades.[4]

Plasmonic nanomaterials such as gold nanoparticles (AuNPs) have very strong light absorption in the visible region because of their so called localized surface plasmon resonance.[5] AuNPs have attracted considerable attention because of their unique physical and chemical properties and their very important applications in catalysis, such as the photocatalytic reduction of organic dyes under visible light irradiation.[5] Gold was considered to be the ‘‘Cinderella’’ of the periodic table for several years and the soul position of the AuNPs were broken by finding its applications in low-temperature CO oxidation.[6,7]

Graphene has attracted remarkable research interest in recent years, owing to its ultrathin, two-dimensional (2D) nature and its surprising properties.[8] Graphene is considered a smart material and it is assumed that in the next decade, it will find commercial applications in many areas ranging from high frequency electronics to smart coatings.[8,9] The unique properties of graphene consist of fast electron transportation, high thermal conductivity, excellent mechanical stiffness and good biocompatibility,[10] which gives it potential applications to composites,[11] field-effect transistors,[12] electromechanical resonators,[13] solar cells,[14] and electrochemical sensors.[15,16] The methods for synthesizing high quality graphene simply include controlling the individual grains and grain boundaries, non-catalytic growth of graphene, low-temperature growth for easy synthesis, and roll-to-roll production of graphene films.[17,18] These outstanding properties of graphene highlight its potential as a

support material to disperse and stabilize metals and metal oxide nanoparticles.[19,20]

Generally, graphene sheets can be dispersed well in alkaline solution but aggregation can occur with any change in the conditions of the solution, such as the addition of salts or acids.[19] Enlightened by these behaviors, considerably more attention has been paid to exploring metal-graphene nanocomposites,[20] such as Au-Graphene.[21,22] Metal nanoparticles have been introduced to graphene because of their extraordinary conductivity and excellent catalytic activity.[23,24] Thus, many approaches for the preparation of Au-G nanocomposite have been attempted, such as chemical reduction processes,[25] physical vapor deposition,[26] hydrothermal techniques,[27] and ex-situ approaches based on weak interaction.[28,29] Although, in these chemical and physical methods, AuNPs can be dispersed over graphene sheets with relatively high density and surface ratios. These processes obviously involve highly toxic chemicals or high temperatures, and complicated manipulations. Some of them might cause contamination in the nanocomposites, thereby reducing the electron transfer capacity and photocatalytic activity.[20] Accordingly, there has been considerable interest and significance in developing a facile, green and environment-friendly strategy for the synthesis of Au-G nanocomposite with improved photocatalytic and photoelectrochemical performance.[6,30] Recently, a series of excellent results with chemical reduction techniques for the synthesis of metal and graphene nanocomposites were reported.[22,23,25,27]

In this study, an electrochemically active biofilm (EAB) was used as a bio-reducing tool and act as an electron supplier for the reduction of Au^{3+} to Au^0 on the surface of graphene sheets. Therefore, the formation of Au-G nanocomposite occurs within 24 h using EAB in the presence of sodium acetate as an electron donor at room temperature.[30-32] This study focused on the one-pot and one-step biogenic synthesis of Au-G nanocomposite using EAB. The present methodology does not involve any hazardous chemicals, expensive oxidizing or reducing agents, hydrothermal treatments and external energy input. This makes the present protocol highly efficient in the field of nanocomposite syntheses, compared to the other methodologies reported elsewhere.[11,20,25] The resulting Au-G nanocomposite was examined for potential applications such as the photocatalytic degradation of organic pollutants under visible light irradiation and enhanced photocurrent measurements. To the best of the author's knowledge, this is the first report using EAB for the synthesis of AuNPs decorated graphene which has been used as a photocatalyst for dye degradation and electrode materials.

Experimental section

Materials

Hydrogen tetracloroaurate (III) hydrate ($HAuCl_4 \cdot nH_2O$; n = 3.7) from Kojima Chemicals, Japan and graphene was purchased from Iljin Nano Tech, Seoul, Korea (7-8 layer graphene sheet with a mean length of 500 nm). Methylene blue (MB) from Sigma-Aldrich and sodium acetate, sodium sulfate (Na_2SO_4) was obtained from Duksan Pure Chemicals Co. Ltd., South Korea. Ethyl cellulose and α-terpineol ($C_{10}H_{18}O$) were acquired from KANTO Chemical Co., Japan. Carbon paper (without wet proof) was supplied by Fuel Cell Earth LLC, USA. All other chemicals used in this study were of analytical grade and used as received. All solutions were prepared from DI water obtained using a PURE ROUP 30 water purification system.

Methods

X-ray diffraction (XRD, PANalytical, X'pert PRO-MPD, Netherland) was carried out using Cu Kα radiation (λ = 0.15405 nm). The XRD peaks of the crystalline phases were compared with those of the standard compounds reported in the JCPDS data file. The optical properties were examined using a UV-VIS-NIR diffuse absorbance/reflectance spectrophotometer (VARIAN, Cary 5000, USA) and photoluminescence (PL, Kimon, 1 K, Japan) of the samples were recorded over the scanning range, 200-800 nm using an excitation wavelength of 325 nm. Raman spectroscopy (Lab Ram HR800 UV Raman microscope; Horiba Jobin-Yvon, France) was also conducted to examine the graphene indepth. X-ray photoelectron spectroscopy (XPS, ESCALAB 250 XPS System, Thermo Fisher Scientific U.K.) was conducted using the following X-ray source: monochromated Al Kα, hν = 1486.6 eV, X-ray energy: 15kV, 150 W and spot size: 500 μm, Take-off angle: 90 degree, Pass energy: 20 eV, BE resolution: 0.6 eV (calibrated by Au 4f 5/2). XPS curve fitting was performed using "AVANTAGE" software by a Shirley subtraction and shape of the peaks used for the deconvolution was a Gaussian-Lorentzian shape. PL and XPS were performed from Korea Basic Science Institute, (KBSI) South Korea. The microstructure was examined by field emission transmission electron microscopy (FE-TEM, Tecnai G2 F20, FEI, USA) operating at an accelerating voltage of 200 kV. Selected-area electron diffraction (SAED) was carried out by TEM. Elemental mapping of the sample containing phases with different valences was obtained by TEM and high angle annular dark field STEM (HAADF-STEM). Quantitative analysis was performed by energy dispersive spectrometry (EDS) attached to the transmission microscope.

The photocatalytic degradation process was monitored by measuring the absorption of organic pollutant at different visible light irradiation times by UV–vis spectrophotometry (OPTIZEN 2120UV) and photoelectrochemical experiment, such as linear sweep voltammetry (LSV) was conducted using a 400 W lamp with an intensity of 31 mW/cm^2 (3M, λ > 400 nm, USA). The LSV measurements were taken using a potentiostat (Versa STAT 3, Princeton Research, USA) comprised of a standard three-electrode system. Ag/AgCl (3 M KCl), a Pt gauge and carbon paper coated with P-G and Au-G nanocomposite, were used as the reference, counter and working photoelectrodes, respectively. The experiment was conducted at room temperature in a 0.2 M Na_2SO_4 solution as the electrolyte. The projection area of the photoelectrode was 1 cm^2. The working electrodes for the photocurrent (LSV) were prepared as follows: 50 mg of each sample was mixed thoroughly by adding ethyl cellulose as a binder and α-terpineol as a solvent for the paste. The paste was then coated on carbon paper using the doctor-blade method.

Preparation of electrochemically active biofilms

The EABs on carbon paper were prepared using the methodology reported elsewhere.[30-33] Briefly, 0.2 g of sodium acetate was added as a substrate to 200 mL of a mineral salt medium. This was followed by the addition of 10 mL of anaerobic sludge (Biogas plant in Paju, Republic of South Korea) and sparging with N_2 gas for 5 min to create strictly anaerobic conditions. Finally, carbon paper (2.5 cm × 4.5 cm) was dipped in the mixture and the bottle was sealed compactly. All media, including the bacterial inoculum were changed every two days under strict anaerobic conditions. The process was repeated for two weeks. The EABs formed on the carbon paper was confirmed using a microbial fuel cell by obtaining the appropriate voltage.[33] The living EABs were employed for the synthesis of the Au-G nanocomposite.

Synthesis of the Au-G nanocomposite using electrochemically active biofilms

In a typical synthesis process, 0.25 g of the graphene sheets was added to 200 mL of an aqueous solution. To this solution, 6 mM gold precursor ($HAuCl_4 \cdot 3.7H_2O$) was added drop-wise to the reaction bottle. The reaction mixture of $HAuCl_4$ and graphene sheets was stirred for 15 min to allow the adsorption of Au^{3+} ions on to the graphene surface. This was followed by addition of 0.2 gm of sodium acetate as an electron donor by sparging N_2 gas for 5 min to maintain an inert atmosphere. The EAB was hung in the reaction bottle, and the bottle was then kept for 24 h with continuous stirring. The EABs produced electrons under anaerobic conditions that were used for the reduction of Au^{3+} ions to Au^0 on to the graphene surface which led to the formation of the Au-G nanocomposite. The isolated Au-G nanocomposite powder was dried in an oven at 60 ^oC for 12 h, and stored in a desiccator until required.

Photocatalytic degradation performance of the Au-G nanocomposite under visible light irradiation

The photocatalytic activity of the as-prepared Au-G nanocomposite and P-G was studied by the photodegradation of MB under visible light irradiation using a 400 W lamp ($\lambda > 400$ nm). 3.0 mg of each photocatalyst (Au-G and P-G) was suspended in 20 mL of an aqueous solution. Each solution was sonicated for 10 min in the dark at room temperature. The solutions were later stirred in the dark for 30 min to reach complete adsorption and desorption equilibrium of the specific substrate. The dye solution was then irradiated with visible light at a working distance of 25 cm. The experiments were observed for 7 h in the case of MB photodegradation experiments. The rate of photodegradation of the dye was monitored by taking 1.7 mL of the samples at every 1 h, centrifuging them to remove the catalyst and recording the UV-vis spectrum. The degradation of the dye was measured as a function of the irradiation time using a UV-vis-spectrophotometer. MB photodegradation was calculated from the decrease in the absorbance of the respective degraded solutions. Each experiment was performed in triplicate under the same conditions to ensure the photocatalytic degradation activity of the Au-G nanocomposite and P-G.

Au-G nanocomposite as photoelectrodes for photocurrent

The photocurrent response of the as-synthesized Au-G nanocomposite and P-G sample were examined by a photoelectrochemical experiment, such as linear sweep voltammetry (LSV), which was carried out under ambient conditions in the dark and under visible light irradiation in 50 mL, of a 0.2 M Na_2SO_4 aqueous solution at room temperature. LSV was first performed in the dark condition and later under visible light irradiation ($\lambda > 400$ nm) at a scan rate of 50 mV/s over the potential range of -0.9 to 0.9 V.

Stability and reusability of the Au-G nanocomposite

The stability of the nanomaterials, such as, Au-G nanocomposite is a major issue of concern. This study examined the stability of the Au-G nanocomposite by sonicating a suspension of the Au-G nanocomposite in water for one hour. The centrifuged solution was then analysed for the leached AuNPs using a UV-visible spectrophotometer. No any AuNPs absorbance peak was observed in the UV-vis spectra.

The reusability of the Au-G nanocomposite was tested three times with the same catalyst in the dye solutions. Approximately 95% of the photocatalytic activity was retained after reuse of three times, revealing the good reusability of the as-prepared nanocomposite as a photocatalyst. This shows that the Au-G nanocomposite was not deactivated significantly.

Results and discussion

Proposed mechanism of environment friendly synthesis of Au-G nanocomposite

The Au-G nanocomposite was prepared using a novel biogenic approach, which is environment-friendly. EABs are a "green" and reductant-free tool, which can be appropriate for this objective.[31] Fig. 1 presents the formation of Au-G nanocomposite using EABs as a bio-reducing tool. EAB provides excess of electrons by biologically decomposing sodium acetate (carbon source) which is used for the reduction of $Au^{3+} \rightarrow Au^0$. These electrons assist in anchoring the AuNPs to the surface of the graphene sheets. The advantage of this protocol is that it does not involve any external energy input or harsh chemicals, which makes this synthesis quite useful and efficient in the field of nanocomposite syntheses. Recently, a series of excellent techniques for the synthesis of metal nanoparticles and metal-metal oxide nanocomposite using EABs are reported.[30,31,33] This is first report for the synthesis of Au-G nanocomposite by EABs. This study highlights the design of a new synthetic route and the preparation of new photocatalyst using SPR of Au and electronic behaviour of graphene. Graphene acts not only as a support for the AuNPs, but also as storage for the electrons produced by the EABs within the arrangement of the carbon atoms. These stored electrons increase dramatically the reduction of gold ions at the surface of the graphene sheets.

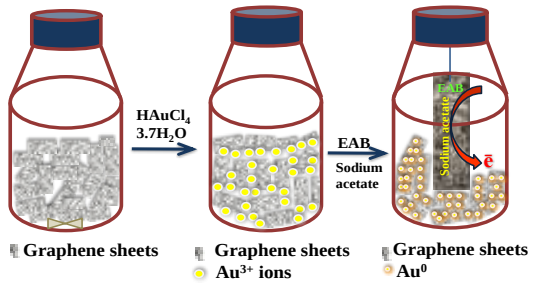

Fig. 1. Proposed schematic model for the synthesis of the Au-G nanocomposites using electrochemically active biofilm.

Optical properties of the P-G and Au-G nanocomposite

The optical properties of the Au-G nanocomposite and P-G were examined by UV-visible absorption spectroscopy and PL. The UV-visible absorption of the as prepared Au-G nanocomposite and P-G was measured at room temperature over the wavelength range, 200–800 nm. Fig. 2 (a) and Fig. S1 presents the typical absorbance and reflectance spectra respectively, indicating the enhanced absorption and reflectance in the case of the Au-G nanocomposite. The absorption spectra (Fig. 2 (a)) of the Au-G nanocomposite showed high absorbance in the range 475-525 nm because of the SPR band characteristic of AuNPs, which shows the presence of AuNPs.[27,34] The reflectance peak (Fig. S1) at 245 nm was shifted to 258 nm in the case of Au-G nanocomposite indicating an electronic conjugation during the reduction of AuNPs by EABs on the graphene sheets.[30,34,35] This further proves the successful formation of the Au-G nanocomposite.

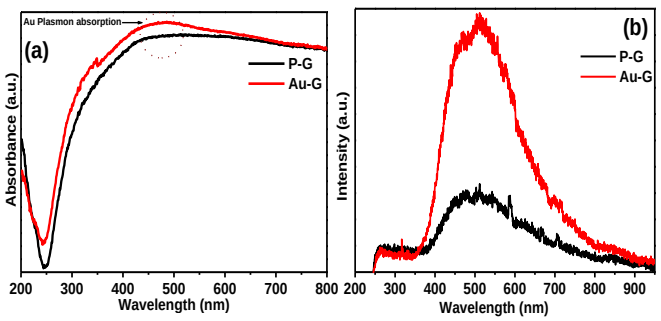

Fig. 2. (a) UV-Vis absorbance spectra, and (b) PL spectra of the P-G and Au-G nanocomposite.

The efficient charge separation and transfer are essential for the enhanced photocatalytic activity of Au-G nanocomposite.[36] Fig 2 (b) shows the PL spectra of the Au-G nanocomposite and P-G at an excitation wavelength of 325 nm. PL shows the emission peaks of P-G at 510 nm in the visible light region, because of the electronic behavior of graphene. In contrast, for the Au-G nanocomposite, the intensity of the emission peak was increased significantly (Fig. 2(b)). This suggests an additional pathway for electron transfer, i.e. from the conduction band of the excited graphene sheets to AuNPs. In general, PL measurements revealed the charge recombination and migration efficiency of the metal and metal oxide nanocomposite, because the photocatalytic activity is associated closely to the PL intensity and the recombination rate of photoexcited electrons and holes.[30] The spectra clearly showed that the excited electron population of graphene decrease due to the anchoring of AuNPs, which suggests that the excited electrons transfer from the excited state of graphene to AuNPs. The only pathway for electron transfer is that the HOMO of the excited AuNPs accepts the electrons from the excited state of graphene.

Structural analysis of the P-G and Au-G nanocomposite

XRD was conducted to confirm the structural changes in Au-G nanocomposite synthesis. The crystalline nature of the Au nanostructures in Au-G nanocomposite was confirmed by XRD, as shown in Fig. 3 (a). The XRD patterns of the Au-G nanocomposite showed the major diffraction peaks at 26.5° (002) and 54.7° (100) for graphene and at 38.1° (111), 44.4° (200), 64.8° (220) and 77.6° (311) for the AuNPs which well match to the face-centered cubic crystalline Au (JCPDS 04-0784).[37] No XRD peaks from other impurities were detected. This clearly shows the successful anchoring of the AuNPs on to graphene sheets.

The mean crystallite size of the Au-G nanocomposite was calculated using the Scherer's formula, $D = \kappa\lambda/\beta\cos\theta$, where, κ is the shape factor and has a typical value of ~ 0.9, λ is the wavelength (Cu Kα = 0.15405 nm), β is the full width at half maximum of the most intense peak (in radians) and θ is the main peak of P-G which was 26.52º. The calculated crystallite size of P-G from the most intense peak at 26.52º 2θ was 22.5 nm and the calculated crystallite size of Au-G nanocomposite from the most intense peak was 26.9 nm. This shows that the crystallite size of Au-G nanocomposite has increased due to the anchoring of AuNPs to the graphene sheets compared to P-G. This further confirmed the successful synthesis of the Au-G nanocomposite.

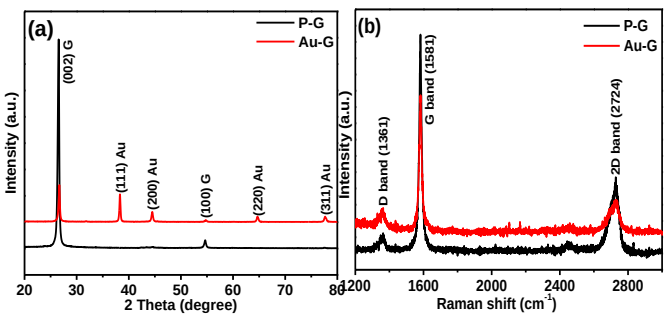

Fig. 3. (a) XRD patterns, and (b) Raman spectra of the P-G and Au-G nanocomposite.

Raman spectroscopy provides valuable information on the structural and electronic properties of graphene.[37,38] Fig. 3 (b) shows the Raman spectra of P-G and the Au-G nanocomposite. The D band (~1361 cm^{-1}) is associated with the defect induced breathing mode of A_{1g} symmetry and the G band (~1581 cm^{-1}) is assigned to E_{2g} symmetry representing the relative degree of graphitization. The 2D band of the Au-G nanocomposite was decreased slightly with respect to P-G, which is consistent with previous reports.[38] The 2D band is well-known as a key parameter to distinguish the thickness of the graphene sheets. In the Au-G nanocomposite a slightly broad 2D

band (2724 cm^{-1}) was observed. The introduction of Au would cause decrease in the intensity of the G and broadening of the 2D band due to electron-phonon coupling.[37] In the present case, the intensity of the G band decreased, which further confirms the anchoring of AuNPs to graphene sheets. The D band of P-G and Au-G was the same, which indicating no defect in the Au-G nanocomposite.[20]

Transmission electron microscopy

Fig. 4 (a) shows a TEM image of the as-prepared Au-G nanocomposite. The AuNPs were almost spherical in shape and dispersed uniformly over the graphene sheets with less aggregation. No free nanoparticles were observed outside the graphene sheets. The transparent and few layer sheets of graphene can be seen in the background. The inset in Fig. 4 (a') shows the SAED pattern which revealed the polycrystalline nature of AuNPs or Au-G nanocomposite. Fig. 4 (b) shows the HR-TEM image which clearly indicates the lattice fringes with a d spacing of approximately 0.235 nm, corresponding to the (111) plane of the face centered cubic (fcc) structure of AuNPs. Furthermore, the interface between the graphene sheets and the AuNPs can be clearly seen. This reveals the strong interaction between the graphene sheets and the AuNPs. The size distribution shows that the AuNPs were relatively uniform with diameters of 10-15 nm. Fig. 4 (c) shows the size distribution histogram, which clearly reveals the average particle size of the AuNPs. This can be attributed to the increase of the active surface area of the AuNPs with the decrease of the size of the catalyst. Fig. 4 (d) and (e) shows the elemental mapping of C-K and Au-M respectively. Fig. S2. shows the HAADF-STEM image of the Au-G nanocomposite for better comparison with the elemental mapping. Fig. S3 presents the result of EDS analysis of Au-G, which showed that the AuNPs were anchored/adsorbed successfully at the surface of the graphene sheets. This was confirmed by EDS analysis of different regions of the Au-G nanocomposite surface as shown in Table S1.

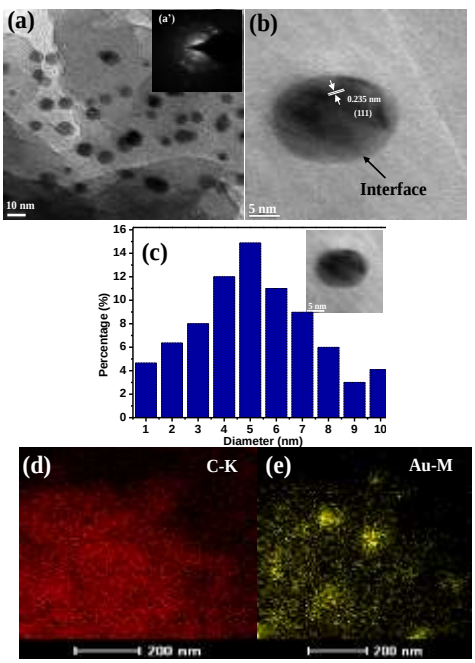

Fig. 4. (a) TEM image and inset (a') showing SAED pattern, (b) HR-TEM image showing the lattice fringes and interface between the graphene sheet and AuNPs, (c) Particle size distribution graph with particle size, (d & e) elemental mapping of the Au-G nanocomposite.

XPS analysis of P-G and Au-G nanocomposite

XPS of as-prepared Au-G nanocomposite and P- G revealed peaks associated with C 1s. Fig. 5 (a) shows the high resolution spectra of the C 1s at characteristic binding energy (B.E.) of 284.4 eV for P-G. In contrast, the C 1s peak for the Au-G nanocomposite shifted to 284.6 eV B.E. which confirms the successful anchoring of AuNPs onto graphene sheets. The inset in Fig. 5 (a') shows the survey spectra of the Au-G nanocomposite in which the peak associated with C 1s became predominant and a peak of Au 4f evidently appeared which shows evidence of the successful decoration of the graphene sheet with AuNPs after being treated with the EAB. In addition, XPS showed no peaks for other elements except for C and Au indicating the high purity of the as-prepared nanocomposite.[30,39] In the high-resolution and fitted XPS spectrum presented in Fig. 5 (b), the Au $4f_{7/2}$ and Au $4f_{5/2}$ peaks were centered at 84.19 eV and 87.89 eV B.E., respectively, which were in agreement with the widely reported XPS spectra of metallic Au^0 at 84.0 eV and 87.7 eV B.E.[39] In addition, the Au^{3+} ions were effectively reduced to Au^0 ions on the surface of the graphene sheets. XPS showed that the Au-G nanocomposite was obtained by the EABs treatment, which shows a strong interaction between the graphene sheets and AuNPs.

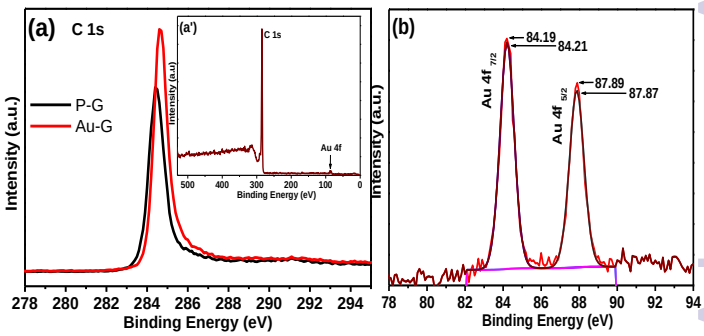

Fig. 5. (a) XPS spectra of C 1s peak, and inset (a') survey scan spectra, and (b) fitting spectra of Au 4f of the Au-G nanocomposite.

Applications of Au-G nanocomposite

Evaluation of the photocatalytic degradation of organic pollutant using Au-G nanocomposite

The photocatalytic activity of the Au-G nanocomposite was evaluated by degrading MB as model pollutant under visible light irradiation, and the results are shown in Fig. 6. MB degradation was enhanced remarkably in the presence of the Au-G nanocomposite as a catalyst. The absorption intensity of MB decreased gradually with increasing irradiation time without a shift of the absorption wavelength. The UV-vis absorption spectra (Fig. 6) showed that the

intensity in the absorption peaks at 246, 292 and 665 nm decreased gradually with increasing reaction time, which is an indication of the photodegradation of MB. Approximately 65% MB was degraded after 7 h, under visible light irradiation in the presence of the Au-G photocatalyst. This suggests that the small size of AuNPs anchored at the surface of the graphene sheets enhanced the photocatalytic activity of graphene for effective pollutant degradation under visible light irradiation. The inset of Fig. 6 shows the photocatalytic degradation kinetics of MB as a function of the irradiation time. Here, C is the absorption of MB solution at each time interval of irradiation, and C_0 is the absorption of the initial concentration (time 0). It was found that in comparison to the earlier studies, the Au-G nanocomposite exhibited quite better visible-light induced photocatalytic degradation of organic pollutants.[27]

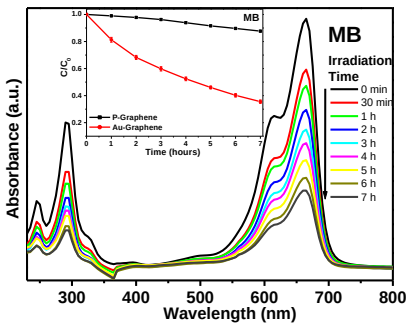

Fig. 6. Visible light-induced photocatalytic degradation of MB using the Au-G nanocomposite.

Mechanism for the photodegradation of MB

Fig. 7 presents the mechanistic profile of the photoinduced charge separation, migration and degradation process under visible light irradiation. A mechanism accounting for the degradation of dye pollutants over Au-G nanocomposite under visible light irradiation is proposed, as illustrated schematically in Fig. 7. Generally, a Schottky barrier is formed when two materials with different work functions are combined, and electrons are transferred from materials with a lower work function to materials with a higher work function until the two levels reach equilibrium to form a new Fermi energy level.[5,6] The equilibrium alignment of the Fermi level of the metal and graphene nanocomposite materials creates a built-in electric field in the space charge region near the interface, which promotes the separation of photogenerated electrons and holes, and enhances the photocatalytic activity.[27]

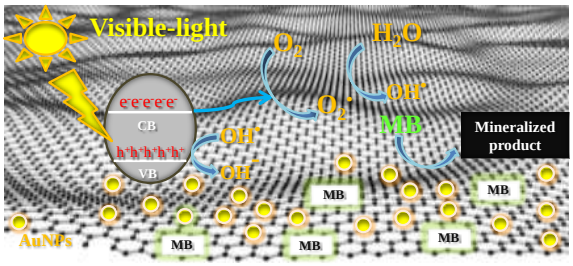

Fig. 7. Proposed mechanism for the photodegradation of MB using the Au-G nanocomposite.

Photocurrent measurements of the Au-G nanocomposite as a photoelectrode

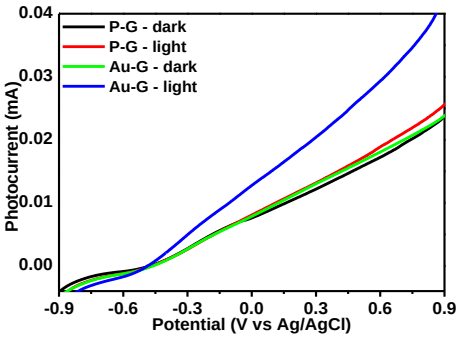

Fig. 8. Photocurrent measurements using LSV for the Au-G nanocomposite as a photoelectrodes in the dark and under visible light irradiation.

Complementary information regarding the photocurrent response of the Au-G nanocomposites was obtained from the linear sweep voltammetry measurements. LSV was performed over the potential range of -0.9 to 0.9 V in the dark and under visible light irradiation to examine the visible light response of the P-G and Au-G nanocomposite for the photocurrent measurements. Fig. 8 shows that the photocurrent measurements of the Au-G nanocomposite increased progressively compared to P-G, which suggests that the anchoring of AuNPs on the graphene sheets can effectively improve the photoconversion efficiency and light harvesting ability of graphene. Generally, an increase in photocurrent suggests that the sample has strong ability to generate and transfer the photoexcited charge carriers under visible light irradiation.[40-42] The increased photocurrent also shows an increase in the transport rate of the photoinduced carriers and an improvement of photogenerated electron-hole pair separation.[30,41,42] This shows the better performance as compared to P-G.

Conclusion

A facile, rapid and environment-friendly biogenic method, using EAB as a bio-reducing tool, was performed for the preparation of an Au-G nanocomposite. The uniformly anchored AuNPs on the surface of the graphene sheets act not only as nucleation sites but also prevent the AuNPs and graphene from agglomeration. The uniform size anchoring of AuNPs, high adsorption ability of graphene and the effective electron transfer from graphene to AuNPs makes the Au-G nanocomposite an efficient catalyst for the photocatalytic degradation of organic pollutants and an effective material for photocurrent. This green and environment friendly approach provides a novel route for the synthesis of nanocomposites with enhanced visible light activities that can be used repeatedly for a range of visible light active applications. Overall, these results show that the Au-G nanocomposite can serve as an effective material for photocatalysis and optoelectronic devices.

Acknowledgement

This study was supported by a 2014 Yeungnam University Research Grant.

Notes and references

[1]*School of Chemical Engineering and* [2]*Center for Research Facilities, Yeungnam University, Gyeongsan-si, Gyeongbuk 712-749, South Korea. Phone: +82-53-810-2517; Fax: +82-53- 810-4631.*
[2]*Chemical Sciences, Faculty of Science, Universiti Brunei Darussalam Jalan Tungku LinK, BE1410, Brunei Darussalam*
****Corresponding Authors Email:** mhcho@ynu.ac.kr; mmansoobkhan@yahoo.com*

†Electronic Supplementary Information (ESI) available: [UV-vis DRS spectra, HAADF, and EDX of Au-G] See DOI: 10.1039/b000000x/

1 H. Zollinger, Synthesis, Properties and Applications of Organic Dyes and Pigments. Color Chemistry, 2nd rev. Edn., VCH, Weinheim, **1991**.
2 R. B. Haveland-Smith and R. D. Combes, *Food Chem. Toxicol.* 1980, **18**, 223–228.
3 T. Yahagi, M. Degawa, Y. Seino, T. Matsushima, M. Nagao, T. Sugimura and Y. Hashimoto, *Cancer Lett.* 1975, **1**, 91–96.
4 C. A. Martı´nez-Huitle and E. Brillas, *Applied Catalysis B: Environmental*, 2009, **87**, 105–145.
5 C. Wang and D. Astruc, *Chem. Soc. Rev.*, 2014, **43**, 7188–7216.
6 H. Chen and L. Wang, *Beilstein J. Nanotechnol.*, 2014, **5**, 696–710.
7 J. Guzman and B. C. Gates, *J. Am. Chem. Soc.*, 2004, **126**, 2672–2673.
8 K. S. Novoselov, V. I. Fal'ko, L. Colombo, P. R. Gellert, M. G. Schwab and Kim K., *Nature*, 2012 , **490**, 192–200.
9 A. K. Geim and K. S. Novoselov, *Nature Materials*, 2007, **6**, 183–191.
10 H. Chen, M. B. Müller, K. J. Gilmore, G. G. Wallace, D. Li, *Adv. Mater.*, 2008, **20**, 3557–3561.
11 S. Stankovich, D. A. Dikin, G. H. B. Dommett, K. M. Kohlhaas, E. J. Zimney, E. A. Stach, R. D. Piner, S.T. Nguyen, R. S. Ruoff, *Nature*, 2006, **442**, 282–286.
12 S. Gilje, S. Han, M. S. Wang, K. L. Wang, R. B. Kaner, A chemical route to graphene for device applications, Nano Lett., 2007, 73394–3398.
13 J. S. Bunch, Z. A. M. Vander, S. S. Verbridge, I. W. Frank, D. M. Tanenbaum, J. M. Parpia, H. G. Craighead, P. L. McEuenh, *Science*, 2007, **315**, 490–492.
14 J. B. Wu, H. A. Becerril, Z. A. Bao, Z. F. Liu, Y. S. Chen, P. Peter, *Appl. Phys. Lett.*, 2008, **92**, 263302.
15 C. S. Shan, H. F. Yang, J. F. Song, D. X. Han, A. Ivaska, L. Niu, *Anal. Chem.*, 2009, **81**, 2378–2382.
16 Y. Wang, Y.M. Li, L.H. Tang, J. Lu, J.H. Li, *Electrochem. Commun.*, 2009, **11**, 889–892.
17 Q. Yu, L. A. Jauregui, W. Wu, R. Colby, J. Tian, Z. Su, H. Cao, Z. Liu, D. Pandey, D. Wei, T. F. Chung, P. Peng, N. P. Guisinger, E. A. Stach, J. Bao, S. S. Pei and Y. P. Chen., *Nature Materials*, 2011, **10**, 443–449.
18 S. Bae, H. Kim, Y. Lee, X. Xu, J. S. Park, Y. Zheng, J. Balakrishnan, T. Lei, H. R. Kim, Y. II Song, Y. J. Kim, K. S. Kim, B. O¨ zyilmaz, J. H. Ahn, B. H. Hong and S. Iijima, *Nature Nanotech.*, 2010, **5**, 574–578.
19 D. Li, M. B. Muller, S. Gilje, R. B. Kaner and G. G. Wallace, *Nat. Nanotechnol*., 2008, **3**, 101–105.
20 P. Wang, Z. G. Liu, X. Chen, F. L. Meng, J. H. Liu and X. J. Huang, *J. Mater. Chem. A*, 2013, **1**, 9189–9195.
21 E. C. Dreaden, A. M. Alkilany, X. Huang, C. J. Murphy and M. A. El-Sayed, *Chem. Soc. Rev.*, 2012, **41**, 2740–2779.
22 R. Muszynski, B. Seger and P. V. Kamat, *J. Phys. Chem. C*, 2008, **112**, 5263–5266.
23 Y. Wang, S. Zhang, D. Du, Y. Y. Shao, Z. H. Li, J. Wang, M. H. Engelhard, J. H. Li and Y. H. Lin, *J. Mater. Chem*., 2011, **21**, 5319–5325.
24 D. Xiaochen, H. Wei, C. Peng, *Nanoscale Res. Lett*., 2011, **60**, 1–6.
25 G. Goncalves, P. A. A. P. Marques, C. M. Granadeiro, H. I. S. Nogueira, M. K. Singh and J. Gracio, *Chem. Mater.*, 2009, **21**, 4796–4802.
26 P. A. Pandey, G. R. Bell, J. P. Rourke, A. M. Sanchez, M. D. Elkin, B. J. Hickey and N. R.Wilson, *Small*, 2011, **7**, 3202–3210.
27 J. Li, C. Y. Liu and Y. Liu, *J. Mater. Chem*., 2012, **22**, 8426–8430.
28 C. Jin, J. Lee, E. Lee, E. Hwang and H. Lee, *Chem. Commun*., 2012, **48**, 4235–4237.
29 Z. Peng, F. Somodi, S. Helveg, C. Kisielowski, P. Specht and A. T. Bell, *Journal of Catalysis*, 2012, **286**, 22–29.
30 M. M. Khan, S. A. Ansari, M. O. Ansari, B. K. Min, J. Lee and M. H. Cho, *J. Phys. Chem. C*, 2014, **118**, 9477−9484.
31 M. M. Khan, S. Kalathil, T. H. Han, J. Lee, and M. H. Cho, *J. Nanoscience and Nanotech.* 2013, **13**, 6079–6085.
32 T. H. Han, M. M. Khan, S. Kalathil, J. Lee and M. H. Cho, *Ind. Eng. Chem. Res.*, 2013, **52**, 8174−8181.
33 M. M. Khan, S. A. Ansari, J. H. Lee, J. Lee, and M. H. Cho, *ACS Sustainable Chem. Eng*. 2014, **2**, 423–432.
34 Y. H. Lee, L. Polavarapu, N. Gao, P. Yuan and Q. H. Xu, *Langmuir*, 2012, **28**, 321–326.
35 Z. Guan, L. Polavarapu, and Q. H. Xu, *Langmuir*, 2010, **26**, 18020–18023.
36 A. Xiaoqiang, Y. C. Jimmy, W. Yu, H. Yongming, Y. Xuelian and Z. Guangjin, *J. Mater. Chem*., 2012, **22**, 8525–8531.
37 J. Song, L. Xu, R. Xing, Q. Li, C. Zhou, D. Liu and H. Song, *Scientific Reports*, 2014, DOI: 10.1038/srep07515.
38 L. G. Cancado, A. Jorio, E. H. Martins Ferreira, F. Stavale, C. A. Achete, R. B. Capaz, M. V. O. Moutinho, A. Lombardo, T. S. Kulmala and A. C. Ferrari, *Nano Lett*., 2011, **11**, 3190–3196.
39 H. J. Yin, H. J. Tang, D. Wang, Y. Gao and Z. Y. Tang, H. J. Yin, H. J. Tang, D. Wang, Y. Gao and Z. Y. Tang, *ACS Nano*, 2012, **6**, 8288–8297.
40 M. M. Khan, S. A. Ansari, D. Pradhan, D. H. Han, J. Lee and M. H. Cho, *Ind. Eng. Chem. Res*., 2014, **53**, 9754−9763.
41 T. Wang, Z. Jiao, T. Chen, Y. Li, W. Ren, S. Lin, G. Lu, J. Ye and Y. Bi, *Nanoscale*, 2013, **5**, 7552–7557.
42 M. M. Khan, S. A. Ansari, M. E. Khan, M. O. Ansari, B. K. Min and M. H. Cho, *New J. Chem.*, 2015, **DOI:** 10.1039/C4NJ02245A.